Luminescence Study of Na6MnCl8 and Na6MnBr8 Microcrystals in NaCl and NaBr Lattices

ARTICLE *in* PHYSICA STATUS SOLIDI (B) · JULY 1994

Impact Factor: 1.49 · DOI: 10.1002/pssb.2221840122

3 AUTHORS, INCLUDING:

Fernando Rodríguez
Universidad de Cantabria
178 PUBLICATIONS **1,325** CITATIONS
SEE PROFILE

Miguel Moreno
Universidad de Cantabria
224 PUBLICATIONS **2,718** CITATIONS
SEE PROFILE

phys. stat. sol. (b) **184**, 247 (1994)

Subject classification: 78.55; 71.70; S9.16

D.C.I.T.T.Y.M. (Sección Ciencia de Materiales), Universidad de Cantabria, Santander[1])

Luminescence Study of Na_6MnCl_8 and Na_6MnBr_8 Microcrystals in NaCl and NaBr Lattices

By

M. C. MARCO DE LUCAS, F. RODRÍGUEZ, and M. MORENO

A detailed study of the luminescence and excitation spectra as well as of the lifetime (τ) on Na_6MnX_8 (X = Cl, Br) precipitates in the 300 to 2 K temperature range is made. In spite of the large distance between nearest Mn^{2+} ions (0.797 nm for Na_6MnCl_8), it is demonstrated that even at 2 K luminescence takes place at excitation traps after an exchange induced transfer between close Mn^{2+} ions. At variance to compounds like MnF_2, only one trap (with depth of 350 and 480 cm^{-1} for X = Cl and Br, respectively) together with killers is mainly responsible for the observed temperature dependence of the luminescence. Aside from the inhomogeneous broadening of the emission band, the extrinsic character of the luminescence is underlined by the experimental Stokes shift observed at 10 K. The analysis of the bandwidth and the vibrational progressions on the $^4T_{1g}(G)$ band is perfectly explained in terms of coupling to the a_{1g} mode. The increase of the Huang-Rhys factor on passing from Na_6MnCl_8, $S(a_{1g}) = 5$, to Na_6MnBr_8, $S(a_{1g}) = 8$, is reasonably explained through a microscopic model. It is demonstrated that the lifetime–temperature dependence is mainly governed by the overlap between the absorption and emission bands. This overlap is estimated subtracting the odd-phonon contribution to the Stokes shift since phonon assistance is not required for excitation transfer through superexchange. The existence of Mn^{2+}–Mn^{2+} transfer down to 2 K is related to the perfect cubic symmetry of these compounds, and to a small coupling to the Jahn-Teller e_g mode. The different thermal shifts experienced by the luminescence and the excitation $^4T_{1g}(G)$ band are also discussed.

1. Introduction

Na_6MnX_8 (X = Cl, Br) crystals displaying the so-called Suzuki-phase structure (Fig. 1) are very attractive for basic research on the following grounds: 1. They exhibit a high symmetry structure (Fm3m space group) in which perfect MnX_6 octahedra do not share any common ligand [1, 2]. 2. The distance between two closest Mn^{2+} ions, R(Mn–Mn), is high compared to that found for other concentrated materials involving Mn^{2+}. For instance R(Mn–Mn) = 0.424 nm for $RbMnF_3$, while X-ray measurements on Na_6MnCl_8 give R(Mn–Mn) = 0.797 nm [2]. In the case of Na_6MnBr_8, R(Mn–Mn) has not been measured but a value close to 0.844 mn can be expected. Therefore, it can be said that these systems exhibit a character which is intermediate between that for concentrated compounds like MnF_2, $RbMnCl_3$, etc. and that for true diluted impurities. 3. All the Na_6MnX_8 crystals studied up to now have been obtained as microcrystalline precipitates in lattices like NaCl or NaBr.

Aside from these relevant aspects, the Suzuki-phase precipitates of Na_6MnBr_8 and, especially of Na_6MnCl_8, have been previously characterized using many experimental techniques: X-ray diffraction [2], electron microscopy [3], neutron scattering [4], magnetic [5, 6] and specific heat [7] measurements, Raman [8, 9], EPR [5], and optical spectroscopy [10 to 12].

[1]) Avd. de los Castros, s/n, E-39005 Santander, Spain.

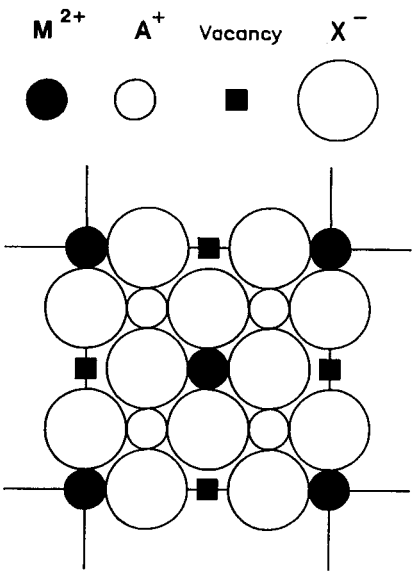

Fig. 1. (100) projection of the unit cell of Na_6MnX_8. The lattice parameter a is just twice that of the NaX lattice

Among the relevant conclusions, such studies reveal that Na_6MnCl_8 becomes antiferromagnetic below $T_N = 0.2$ K in qualitative agreement with $R(Mn-Mn) = 0.797$ nm and the long superexchange pathway involving at least two Cl^- ions [6, 7]. Along this line, susceptibility measurements and the analysis of the EPR bandwidth lead to $J = -0.017\ cm^{-1}$ [5], where the effective exchange interaction occurs only between closest Mn^{2+} ions and can be written as $H_{ex} = -J \sum_{i>j} \boldsymbol{S}_i \cdot \boldsymbol{S}_j$. A similar value, $J = -0.014\ cm^{-1}$, was inferred for Na_6MnBr_8 from the experimental EPR bandwidth [14]. Furthermore for the Suzuki-phase precipitates formed in $NaCl:Mn^{2+}$, evidence of size effects was found in the susceptibility data below 0.3 K [6].

Having in mind these previous results, through the present work we aim to perform a detailed investigation on the luminescence properties of Na_6MnX_8 (X = Cl, Br). In fact, the investigations carried out up to the present have mainly been focused on excitation spectroscopy [10 to 12, 14], but luminescence as well as its time dependence remain still unexplored. A first goal is to determine the kind of luminescence detected in Na_6MnX_8 (X = Cl, Br) that was firstly reported in [10 to 12, 14]. In other words, we like to explore whether the observed luminescence is intrinsic, or in contrast, arises from a trap after a migration process in spite of the long $R(Mn-Mn)$ distance. Since the latter mechanism will be shown to be the correct one, the nature of the migration process is fully analyzed. In particular, an attempt is made to correlate quantitatively the temperature dependence of the lifetime τ with the corresponding overlap between absorption and emission bands.

In this regard, attention is paid to the understanding of the differences between the $^6A_{1g}(S) \rightarrow {}^4T_{1g}(G)$ excitation band and the corresponding emission band. In particular, the former band exhibits at low temperature a well resolved vibrational structure which is totally absent in the luminescence spectrum. Finally, efforts are devoted to analyze the origin of such vibrational structure and to measure the corresponding Huang-Rhys factors which are subsequently related to the experimental Stokes shift and the odd-mode frequencies enabling an electric dipole character to the crystal-field transitions of the MnX_6 octahedron.

Following recent results reported in [15], an attempt is also made to correlate the experimental Huang-Rhys factor, $S(a_{1g})$, associated with the symmetric mode, to $\partial E_1/\partial R$, where E_1 denotes the energy of the $^6A_{1g}(S) \rightarrow {}^4T_{1g}(G)$ transition and R is the ligand–Mn^{2+} distance.

2. Experimental Details

The $NaCl:Mn^{2+}$ and $NaBr:Mn^{2+}$ single crystals containing Suzuki-phase precipitates which are investigated in this work are the same ones used in [4] and [14], respectively. The

$NaCl:Mn^{2+}$ samples contain 5000 ppm of Mn^{2+}; the Suzuki-phase precipitates display nearly cube shapes with 500 nm edge length. The Mn^{2+} concentration in the $NaBr:Mn^{2+}$ is 500 ppm.

Excitation spectra were obtained through a modified [16] Jobin Yvon JY3D fluorimeter. Luminescence was induced by excitation with a Spectra Physics 162 A-07 Ar laser operating at 514 nm and 15 mW, and dispersed by a Jobin Yvon HR 320 monochromator. A Hamamatsu R-928 photomultiplier and a Stanford System SR400 pre-amplifier and SR440 photon counter were employed for signal detection. For lifetime measurements the exciting laser beam was modulated with a mechanical chopper and the luminescence signal was digitized with a Tektronix 2430A scope. Suitable programs for spectral moment and decay analysis were developed.

For temperatures between 10 and 300 K we used a Scientific Instruments Displex DE-202 closed-circuit cryostat with a APD-K controller. This allowed temperature stabilizations to within 0.1 K. Luminescence experiments between 2 and 10 K were performed with an Oxford CF 1204 helium flow cryostat.

3. Results

Fig. 2 shows the excitation and luminescence spectra of $NaCl:Mn^{2+}$ and $NaBr:Mn^{2+}$ crystals containing Suzuki-phase precipitates at 300 K and lower temperatures. The excitation spectra of both systems coincide with those previously reported [10, 11, 14]. Six excitation peaks corresponding to d^5 intraconfigurational transitions from the $^6A_{1g}(S)$ ground state to the excited spin quartets are clearly observed.

The 300 K luminescence spectra consist of one single broad band peaking at 600 nm in both systems. On cooling from 300 to 10 K, these bands experience a continuous red shift of 600 and 530 cm^{-1} in Na_6MnCl_8 and Na_6MnBr_8, respectively (Fig. 3a) as well as an increase by one order of magnitude in the luminescence intensity (Fig. 4). It is worth stressing that luminescence red shifts are much greater than those displayed by the corresponding $^4T_{1g}(G)$ excitation bands which are 150 and 250 cm^{-1}, respectively.

The temperature dependences of the luminescence lifetime, τ, and the bandwidth, H, derived from the second order moment of the band, M_2, through the formula $H = 2.36\sqrt{M_2}$, are depicted in Fig. 4 and 3b, respectively.

The lifetime values for Na_6MnCl_8 were obtained by exponential fitting of the luminescence decay curve, $I(t)$, for times longer than 0.1τ after ceasing excitation, where $I(t)$ behaves as a single exponential in the whole temperature range. Small departures from this behaviour are found for $t < 0.1\tau$. The results collected in Fig. 4 point out that the experimental lifetime, τ, experiences a significant decrement upon warming above about 80 K, which is followed by a parallel decrease of the luminescence intensity. So, for instance, for Na_6MnCl_8 $\tau = 70$ ms at 10 K while $\tau = 4$ ms at 300 K. We have verified that the measured τ is the same for the wavelengths included in the emission band.

In Na_6MnBr_8, the lifetime varies from 9 ms at 300 K to 25 ms at 10 K. However, the luminescence–time dependence is rather complex above 90 K. At this temperature the decay curve leaves the single exponential behaviour and a new slow component is observed in the decay tail. The fast low-temperature component progressively decreases in intensity and lifetime with increasing temperature, and the new slow component dominates the whole decay above 170 K, with τ values varying from 15 ms at 170 K to 9 ms at 300 K. The lifetime data (Fig. 4) in the range 90 to 200 K were obtained by fitting the $I(t)$ decay to the sum

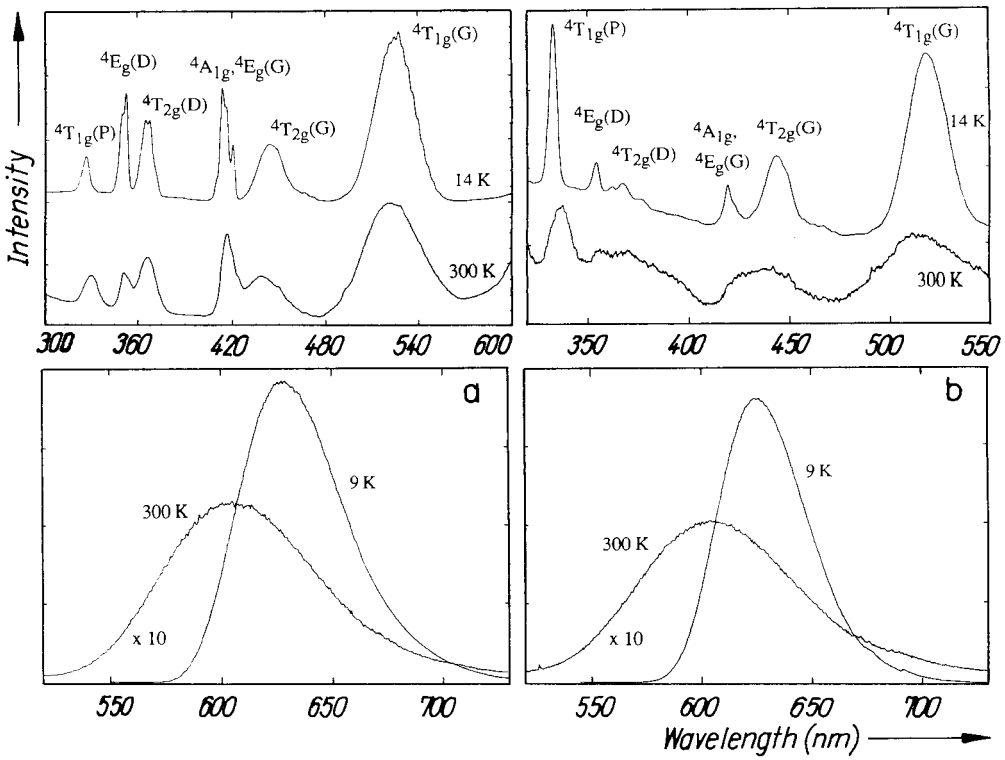

Fig. 2. Excitation (upper parts) and luminescence (lower parts) spectra of a) Na_6MnCl_8 and b) Na_6MnBr_8 precipitates at 300 K and lower temperatures. The excitation spectra were recorded by monitoring the luminescence at 633 nm. Spectral resolution $\Delta\lambda = 2$ nm. The luminescence spectra were recorded under the following conditions: delay time 0.5 ms, counting time 10 and 30 ms for $T = 300$ and 9 K, respectively

of two single exponentials. This fitting successfully reproduces the luminescence–time dependence.

A noticeable fact of the present results concerns the high values of the low-temperature lifetime, $\tau = 70$ and 25 ms, found in Na_6MnCl_8 and Na_6MnBr_8, respectively, which are the longest ones measured for Mn^{2+} in chlorides and bromides, the former one being similar to those found for Mn^{2+} in fluoride lattices ($\tau \approx 100$ ms) [17 to 20].

The appearance of the slow decay component above 90 K in Na_6MnBr_8 just as the luminescence intensity decreases, is also evidenced by changes in the variations undergone by both the first moment and the bandwidth of the Na_6MnBr_8 emission band with temperature (Fig. 3). Such variations indicate that the low-temperature luminescence is placed about 200 cm^{-1} above the extrapolated energy corresponding to the emission band associated to the slow high-temperature component decay. None of these variations has been observed through the corresponding excitation spectrum which remains unaffected over this temperature range.

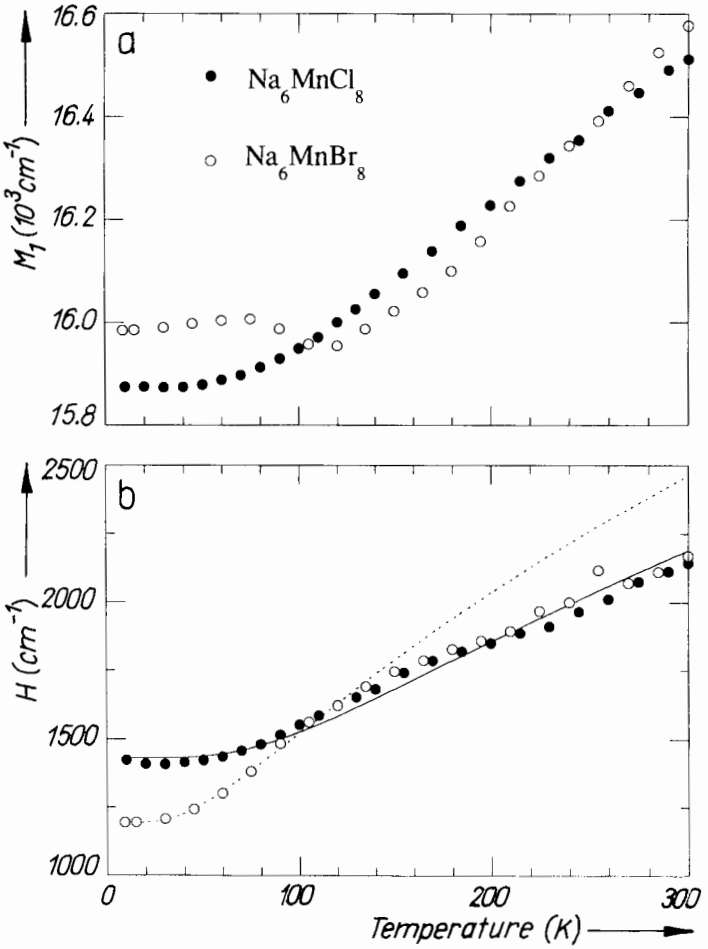

Fig. 3. Temperature dependence of a) the first moment, M_1, and b) the luminescence bandwidth, H, for Na_6MnCl_8 and Na_6MnBr_8. The bandwidth values were derived from the second moment, M_2, through $H = 2.36\sqrt{M_2}$. Full and dotted lines in b) represent the fittings to (1) in the 9 to 300 K range for Na_6MnCl_8, and in the 9 to 100 K range for Na_6MnBr_8, respectively

The experimental variations of the luminescence bandwidth with temperature are compared with those given by

$$H(T) = H(0)\left[\coth\left(\frac{\hbar\omega_{\text{eff}}}{2kT}\right)\right]^{1/2}. \tag{1}$$

The values $H(0) = 1430$ and $1200\,\text{cm}^{-1}$, and $\hbar\omega_{\text{eff}} = 190$ and $100\,\text{cm}^{-1}$, were used for Na_6MnCl_8 and Na_6MnBr_8, respectively, in Fig. 3b. The thermal broadening of the corresponding excitation bands is also explained with (1) but using slightly different frequencies: $\hbar\omega_{\text{eff}} = 214$ and $130\,\text{cm}^{-1}$ respectively. These frequencies are very similar to

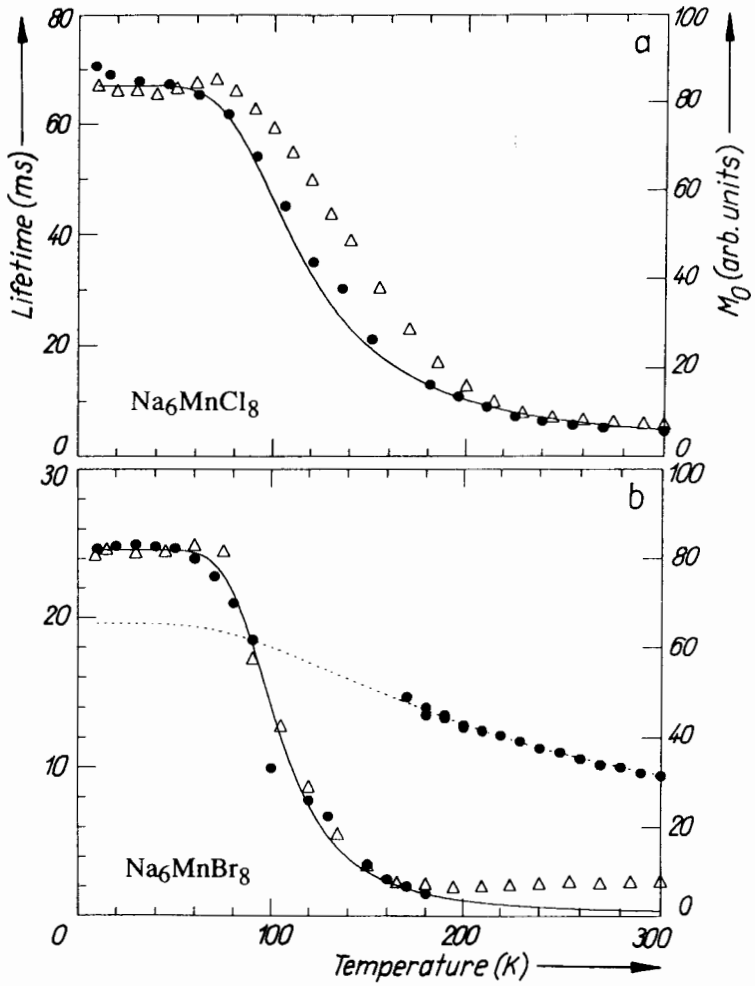

Fig. 4. Temperature dependences of the lifetime (●) and integrated intensity M_0 (△) of the luminescence for a) Na_6MnCl_8 and b) Na_6MnBr_8. In the 90 to 200 K range the luminescence–lifetime dependence of the Na_6MnBr_8 precipitates behaves as the sum of two single exponential decays whose corresponding lifetimes are given in b). Full lines represent the fittings to (4) (see text). Dotted line depicts the calculated lifetimes τ_R^* using (14) with the following parameters: $\tau_R^*(0) = 19.5$ ms and $\hbar\omega_u = 220\ cm^{-1}$

those reported for the a_{1g} vibrational mode by Raman spectroscopy [8, 13]. The values of $H(0)$ for the excitation band were found to be equal to 1100 and 800 cm^{-1} for Na_6MnCl_8 and Na_6MnBr_8, respectively.

Coupling to vibrations is clearly seen in the case of the $^6A_{1g}(S) \rightarrow {}^4T_{1g}(G)$ excitation band as depicted in Fig. 5. These results, which are consistent with previously reported data [11, 14], are discussed in the following section. By contrast, no vibrational structure is resolved in the corresponding emission spectra down to 2 K.

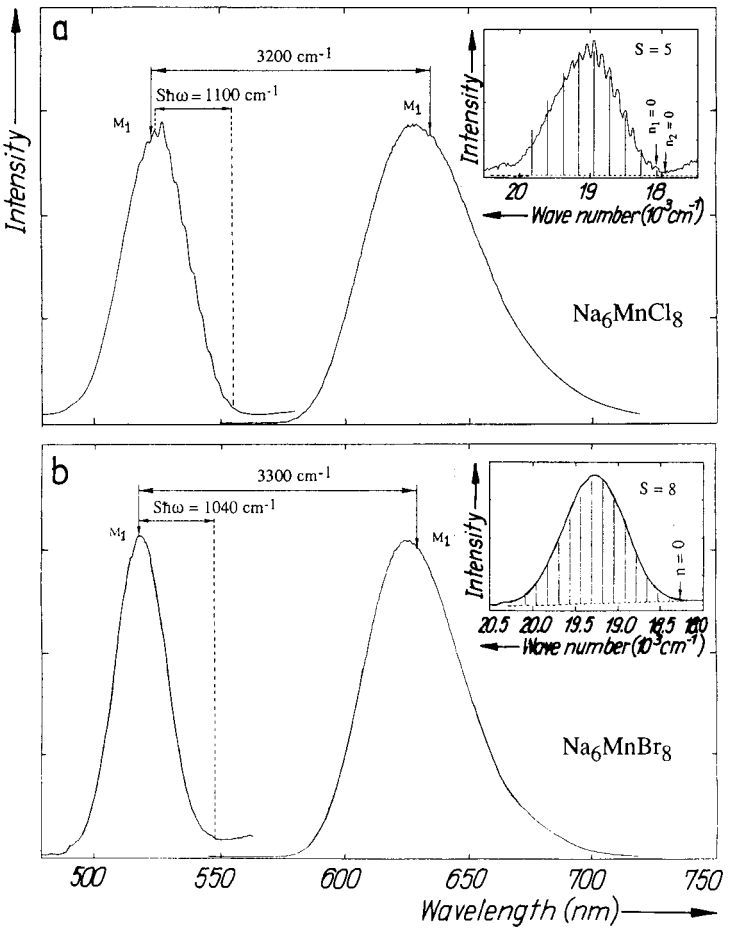

Fig. 5. Low-temperature $^4T_{1g}(G)$ excitation band and luminescence spectra of a) Na_6MnCl_8 and b) Na_6MnBr_8. Vertical arrows indicate the position of the first moment, M_1, of both bands. The insets show a magnification of the excitation band (spectral resolution, $\Delta\lambda = 0.2$ and 2.0 nm for a) and b), respectively). Vertical lines represent the intensity given by the Pekarian distribution, $I = I_0 S^n/n!$, using the following parameters: a) $S = 5$ and $\hbar\omega = 220\ cm^{-1}$ (the intensity is drawn for only one progression); b) $S = 8$ and $\hbar\omega = 130\ cm^{-1}$

4. Discussion

Having in mind all our goals, we have divided the present discussion in four sections for the sake of clarity.

4.1 Vibronic coupling

The vibronic structure displayed by the first excitation band at 9 K in Na_6MnCl_8 (Fig. 5a) and Na_6MnBr_8 (Fig. 5b) was previously explained in terms of progressions of the totally symmetric a_{1g} mode [11, 14]. However, it is worth pointing out that while the progression

in Na_6MnBr_8 is clearly due to the a_{1g} mode, such an assignment in Na_6MnCl_8 involving two 220 cm^{-1} replicas, just separated by 110 cm^{-1}, seems questionable. Moreover, if we consider that a linear coupling of the $^4T_{1g}(G)$ electronic state to the lower frequency e_g or t_{2g} Jahn-Teller modes may exist in terms of symmetry grounds, then the existence of progressions to such modes must not initially be ruled out. In any event, the present experimental results, as well as their comparison to other Mn^{2+} complexes, strongly support the notion that the vibronic couplings mainly involve the a_{1g} mode. The arguments are the following:

1. The Na_6MnCl_8 lattice has two modes of t_{2g} symmetry whose frequencies, 187 and 132 cm^{-1}, determined by Raman scattering [8, 9] cannot account for the observed progression.

2. The e_g mode has not been detected by Raman scattering, neither in Na_6MnCl_8 nor Na_6MnBr_8, but it was seen in Suzuki-phase precipitates formed in Ni-doped LiCl [21] and NaCl [22] with frequencies $\hbar\omega_{e_g} = 161$ and 136 cm^{-1}, respectively. These values are always higher than one half of the corresponding a_{1g} frequencies: 224 and 223 cm^{-1}, respectively.

3. The assignment to two a_{1g} replicas in Na_6MnCl_8 leads to a value of $\hbar\omega_{a_{1g}} = 220$ cm^{-1} slightly higher than that of 214 cm^{-1} measured by Raman scattering at 77 K [8]. This hardening of the a_{1g} force constant in the excited state reflects a decrease in the Mn^{2+}–Cl^- bond distance as it is expected for the $^4T_{1g}(G)$ state mainly involving the t^4e configuration [23].

4. The $^4T_{1g}(G)$ excitation band shape (inset of Fig. 5) is well reproduced with an average Huang-Rhys parameter $S(a_{1g}) = 5$ for both progressions in Na_6MnCl_8, and $S(a_{1g}) = 8$ in Na_6MnBr_8. If we assume only one e_g progression of 110 cm^{-1} in Na_6MnCl_8, the band shape could not be so well reproduced with the corresponding Huang-Rhys parameter $S(e_g) = 11$. In particular, the second moment for this band at 9 K, $M_2 = 2.2 \times 10^5$ cm^{-2}, must be compared with those expected on the basis of two 220 cm^{-1} a_{1g} or one 110 cm^{-1} e_g progressions,

$$M_2(a_{1g}) = [S(a_{1g}) + 1/8]\,(\hbar\omega_{a_{1g}})^2 = 2.5 \times 10^5\ cm^{-2},$$

$$M_2(e_g) = S(e_g)\,(\hbar\omega_{e_g})^2 = 1.3 \times 10^5\ cm^{-2}$$

for $S(a_{1g}) = 5$ and $S(e_g) = 11$. The $S(a_{1g})$ value is increased by 1/8 to take into account the two displaced progressions.

5. The effective frequencies, $\hbar\omega_{eff}$, obtained from the temperature dependence of the bandwidth are 190 cm^{-1} (emission) and 214 cm^{-1} (excitation), the latter value being equal to the Raman a_{1g} frequency.

6. Finally, it must be noted that most vibronic replicas observed in the optical spectra of octahedral transition-metal complexes, such as Ni^{2+} or Mn^{2+}, correspond to a_{1g} vibronic modes with the exception of Cr^{3+} and V^{2+}, where besides a_{1g}, nice e_g progressions have been observed in chloro- [24] and fluoroelpasolites [25 to 27]. In the particular case of Mn^{2+}, a salient feature of the present results concerns the observation of a_{1g} replicas in the $^4T_{1g}(G)$ band. In fact, a_{1g} progressions have occasionally been observed but made upon other crystal field bands. Only $MnCl_2$ crystals are known to show a_{1g} progressions in the $^4T_{1g}(G)$ excitation band [28] though they are reported to be very weak. By contrast, they appear in the $^4T_{2g}(G)$, $^4A_{1g}{}^4E_g(G)$, and $^4T_{2g}(D)$ in MnX_2 [28], $CdX_2:Mn^{2+}$ [29], and $CsCdX_3:Mn^{2+}$ [30] for X = Cl and Br, and NH_4MnCl_3 [31]. It is worthy to point out that progressions of e_g and t_{2g} vibrational modes have never been observed in the $^6A_{1g}(S) \rightarrow {}^4T_{1g}(G)$ transition of either $MnCl_6^{4-}$ or $MnBr_6^{4-}$.

Though the $110\,cm^{-1}$ energy difference between the a_{1g} progressions in Na_6MnCl_8 precipitates was attributed to different spin–orbit components of the $^4T_{1g}(G)$ state in [11], we actually suggest that each progression is made up from a distinct electric-dipole (ED) false origin associated with two different t_{1u} or t_{2u} odd parity vibrations. In fact, the spin–orbit splitting between the extreme Γ_6 and Γ_7 spinors should not be larger than $150\,cm^{-1}$ in $MnCl_6^{4-}$ complexes [32] even if the Ham effect was absent. In particular, the spin–orbit splitting in the $^4T_{1g}(G)$ state of Mn^{2+} in $KMgF_3:Mn^{2+}$ and $KZnF_3:Mn^{2+}$ has recently been detected through the luminescence spectra. The separation between Γ_7 and the highest Γ_8 is smaller than $20\,cm^{-1}$, associated to $S(e_g) = 1.5$ [19].

In the case of Na_6MnB_8 the experimental value $H(0) = 880\,cm^{-1}$ at 9 K for the $^4T_{1g}(G)$ excitation band leads to $M_2 = 1.39 \times 10^5\,cm^{-2}$. This value is only a little higher than the contribution due to the a_{1g} mode alone, $S(a_{1g})\,\hbar\omega^2(a_{1g})$, which is equal to $1.35 \times 10^5\,cm^{-2}$. The small difference could be compatible with an Huang-Rhys factor, $S(e_g)$, for the e_g mode close to unity.

Following recent ideas [15] let us now discuss the microscopic origin of the Huang-Rhys factor $S(a_{1g})$ observed for the $^4T_{1g}(G)$ excitation band of both Na_6MnX_8 (X = Cl, Br) compounds. By virtue of the special structure displayed by the Suzuki phase, the a_{1g} mode of the MnX_6 complex is also a lattice mode. If we denote by E the energy of a given optical transition corresponding to a complex embedded in a lattice, $S(a_{1g})$ is related to $(\partial E/\partial R)_{R_s}$ and thus to the dependence of E upon the metal–ligand distance keeping the surrounding atoms to the complex fixed. R_s symbolizes the position of such surrounding atoms. Therefore, the quantity $(\partial E/\partial R)_{R_s}$ is not necessarily the same as $(\partial E/\partial R)_l$ calculated for an isolated complex unless the electronic potential, V_r, created by the rest of the lattice upon the complex is perfectly flat for every R value attainable during the motion due to the a_{1g} vibration. The influence of the non-flatness of V_r upon $10Dq$ of CrF_3 and K_2NaCrF_6 has recently been discussed [33]. Important effects appear when the 3d ion occupies an interstitial position as it happens for $NH_4Cl:Cu^{2+}$ (II) [34].

The expression for $S(a_{1g})$ in terms of $(\partial E/\partial R)_{R_s}$ is, for an octahedral complex, as follows [15]:

$$S(a_{1g}) = \frac{1}{12\hbar M\omega_{a_{1g}}^3}\left(\frac{\partial E}{\partial R}\right)_{R_s}^2, \tag{2}$$

where M stands for the ligand mass.

In order to apply (2) to the $^4T_{1g}(G)$ excitation band, with an energy E_1, it is necessary to know $(\partial E_1/\partial R)_{R_s}$. It can be estimated from the reported values $(\partial E_1/\partial P) = -26 \times 10^{-8}\,cm^{-1}/Pa$ and $-30 \times 10^{-8}\,cm^{-1}/Pa$ for $MnCl_2$ and $MnBr_2$ [35], respectively, assuming that E_1 only depends on the metal–ligand distance, R, of the corresponding MnX_6^{4-} (X = Cl, Br) complex and so $(\partial E/\partial R)_{R_s}$ is independent of R_s.

Furthermore, taking into account that the bulk modulus, B, for MnF_2 is equal to 880×10^8 Pa [36] and thus assuming $B(MnCl_2) = 500 \times 10^8$ Pa and $B(MnBr_2) = 420 \times 10^8$ Pa, the following estimations are obtained: $(\partial E_1/\partial R) = 150\,cm^{-1}/pm$ for $MnCl_6^{4-}$, and $(\partial E_1/\partial R) = 137\,cm^{-1}/pm$ for $MnBr_6^{4-}$.

Now putting these values into (2) and using the experimental $\hbar\omega(a_{1g}) = 214\,cm^{-1}$ for Na_6MnCl_8, and $\hbar\omega(a_{1g}) = 132\,cm^{-1}$ for Na_6MnBr_8, we arrive at the following estimations: $S(a_{1g}) \approx 2$ and $S(a_{1g}) \approx 3$ for Na_6MnCl_8 and Na_6MnBr_8, respectively.

These values are in agreement with the observed increase of $S(a_{1g})$ on going from the chloride lattice to the bromide one. A similar situation has been encountered for Cr^{3+} in

different elpasolite-type lattices [24, 37] and it is discussed in [15]. Although the estimated ratio between the two Huang-Rhys factors $S(a_{1g})$ is close to the experimental one, the values themselves are smaller than the experimental ones. Values of $(\partial E_1/\partial R)_{R_e}$ close to 210 cm^{-1}/pm could account, however, for the experimental facts.

4.2 Nature of the observed luminescence

The thermally induced non-radiative phenomena observed through the temperature dependences of the lifetime, τ, and the luminescence intensity (Fig. 4) can hardly be explained on the basis of a multiphonon relaxation process. In fact, such a non-radiative mechanism is expected to be negligible in this temperature range for $MnCl_6^{4-}$ since the number of vibrational quanta required to bridge an energy gap of 17000 cm^{-1} is about 80 if the totally symmetric a_{1g} mode was involved. The situation is much more drastic for $MnBr_6^{4-}$. The variation of $\tau(T)$ due to this process has been successfully explained in terms of only one effective mode for $NiCl_6^{4-}$ [38], NiF_6^{4-} [39], CrF_6^{3-} [40], VF_6^{3-} [41], etc., following the procedure of Sturge [42]: $\tau^{-1}(T) = \tau_R^{-1}(T) + \tau_{NR}^{-1}(T)$, where τ_R^{-1} is the radiative rate and τ_{NR}^{-1} is given by

$$\tau_{NR}^{-1}(T) = \tau_{NR}^{-1}(0)\, e^{-2S}\, p!\, S^{-p} \left(\frac{n+1}{n}\right)^{p/2} I_p(2S\sqrt{n(n+1)}), \tag{3}$$

where $\tau_{NR}^{-1}(0) = P_0\, e^{-S}\, S^p/p!$ is the non-radiative rate at 0 K. P_0 contains the electronic matrix element of the interaction, and $e^{-S}\, S^p/p!$ is the Franck-Condon factor at 0 K, p is the number of quanta for bridging the energy gap between the ground and excited electronic states, $n = [\exp(\hbar\omega/kT) - 1]^{-1}$ is the Bose-Einstein occupancy, and $I_p(x)$ the modified Bessel function.

In the case of Na_6MnCl_8 precipitates, this expression is not able to reproduce the experimental $\tau(T)$ behaviour given in Fig. 4 even for vibrational frequencies larger than 250 cm^{-1}, taking as in usual cases $\tau_{NR}^{-1}(0)$ as a fit parameter. Fig. 6a shows the lifetime variation within this model.

By contrast, the temperature dependence of τ is well described by

$$\tau^{-1}(T) = \tau^{-1}(0) + p \exp(-\Delta/kT), \tag{4}$$

characteristic of thermally activated processes.

The full curves in Fig. 4 correspond to the following parameters: $\Delta = 350$ and 480 cm^{-1}, $\tau^{-1}(0) = 14.9$ and 14.7 s^{-1}, and $p = 10^3$ and 5×10^4 s^{-1} for Na_6MnCl_8 and Na_6MnBr_8, respectively. The $\tau(T)$ behaviour of the slow component in $NaBr:Mn^{2+}$ in the 150 to 300 K temperature range follows the law characteristic of phonon-assisted ED transitions [17, 43]: $\tau(0)\tanh(\hbar\omega_u/2kT)$. Values of $\tau(0) = 19.5$ ms and $\hbar\omega_u = 220$ cm^{-1} were used in Fig. 4b.

The preceding arguments strongly support the idea that the temperature dependence of the lifetime τ can be associated with a trap luminescence preceded by a migration process as the mechanism responsible for the observed luminescence. The strong decrease experienced by τ and the luminescence intensity above 80 K should then be associated with the progressive depopulation of traps and the subsequent transfer to killers. In other words, the character of the luminescence is extrinsic in the whole investigated temperature range. Nevertheless, this character is, in principle, not easy to reconcile with the experimental blue shift experienced by the emission peak upon heating. In fact, such a behaviour is opposite to the typical one found in most Mn^{2+} concentrated material such as pure MnF_2 [18, 20, 44],

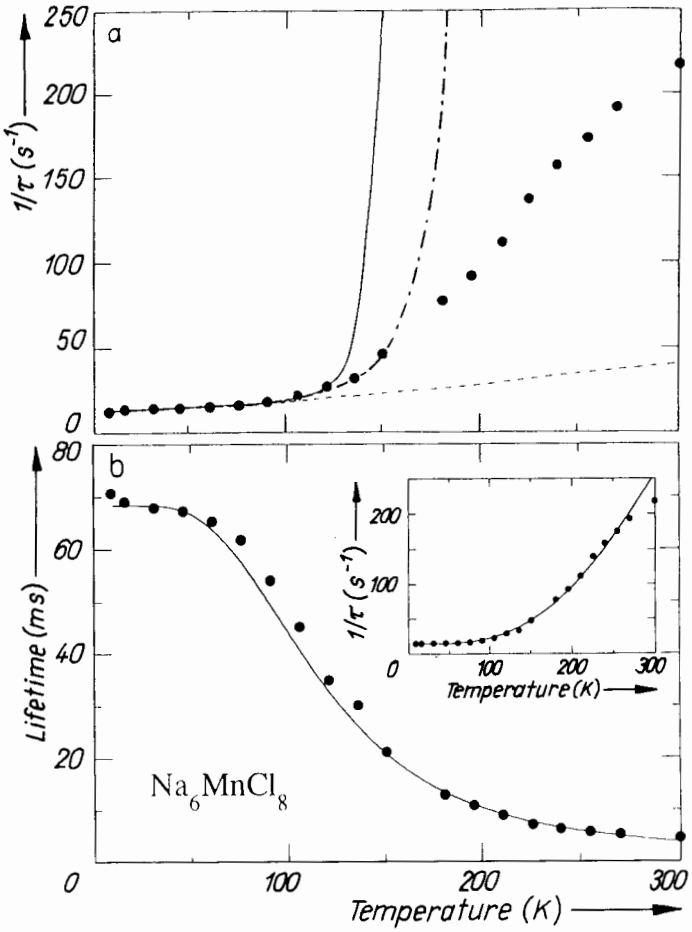

Fig. 6. Temperature dependence of the lifetime in the 9 to 300 K range for Na_6MnCl_8. Points represent the experimental data. a) Curves depict the theoretical transition rates taking into account multiphonon relaxation processes: $\tau^{-1}(T) = \tau_R^{-1}(T) + \tau_{NR}^{-1}(T)$, with $\tau_R^{-1}(T)$ and $\tau_{NR}^{-1}(T)$ as given in (14) and (3), respectively. Dashed line represents $\tau_R^{-1}(T)$ with $\tau_R^{-1}(0) = 14.5\ s^{-1}$ and $\hbar\omega_u = 300\ cm^{-1}$. Full and dashed-dotted lines have been calculated including the non-radiative rate using the following parameters: $\tau_{NR}^{-1}(0) = 0.05\ s^{-1}$, $\hbar\omega_{eff} = 190\ cm^{-1}$, $S = 6.6$, $p = 92$ and $\tau_{NR}^{-1}(0) = 0.9\ s^{-1}$, $\hbar\omega_{eff} = 290\ cm^{-1}$, $S = 4.3$, $p = 60$, respectively. b) Calculated $\tau(T)$ curve considering that the temperature dependence is mainly governed by the overlap between emission and excitation bands (17). The solid line corresponds to the following fitting parameters: $\tau_R^{-1}(0) = 7.8\ s^{-1}$, $A = 3500\ s^{-1}$ $[\Delta E^*/H_{1/2}(0)]^2 = 24$, $\hbar\omega_u = 300\ cm^{-1}$, and $\hbar\omega_{eff} = 214\ cm^{-1}$. The inset depicts the reciprocal lifetime values

$RbMnF_3$ [18], Rb_2MnCl_4 [45, 46], or Mn^{2+} precipitates in $RbCl:Mn^{2+}$ [47], $LiF:Mn^{2+}$ [48] or $KBr:Mn^{2+}$ [49], whose luminescence peaks shift to lower energies as the temperature increases due to migration and subsequent energy transfer to Mn^{2+} shallow traps. This way, the continuous red shift observed in MnF_2, from 4 to 120 K is explained in terms of a progressive thermal depopulation of shallower traps followed by transfer to deeper ones. The luminescence quenching above 120 K is finally attributed to energy transfer to killers of excitation, i.e. non-luminescent impurities. Such a mechanism leads to lifetime dependences

as those given by (4). The activation energy, Δ, represents the trap depth and p is the Mn^{2+} trap–Mn^{2+} transfer rate.

The present experimental results can be understood, however, assuming that in our case only one kind of trap is dominant. This is at variance with the findings for compounds like MnF_2. The blue shift experienced by the first moment of the emission band upon heating is thus consistent with the normal behaviour characteristic of an isolated complex, reflecting but partially the decrease of $10Dq$ and thus the corresponding increase of E_1. A detailed discussion on this point is given in [50] and [51].

Although the present analysis on $\tau(T)$ is consistent with the existence of an excitation transfer process, it is in principle not easy to understand at low temperature where the overlap between the emission and the $^4T_{1g}(G)$ band is practically negligible. A detailed analysis on this process is offered in Section 4.4.

Before ending this section, let us mention that the slow component of the NaBr:Mn^{2+} luminescence following a tanh $(\hbar\omega_u/2kT)$-type behaviour could actually be ascribed either to isolated Mn^{2+} centres, out of the Suzuki phase, or to deeper Mn^{2+} traps which could not transfer back to the other Mn^{2+} ions and thus the corresponding luminescence would present a predominantly intrinsic character. This latter possibility seems to be more convincing taking into account that the excitation spectrum does not change in the same way as the luminescence does. The red shift of about 200 cm^{-1} observed in Fig. 3a would indicate a trap of about 700 cm^{-1}.

4.3 Stokes shift

The Stokes shift, ΔE_S, corresponding to an octahedral MX_6 complex (M transition-metal ion) placed in a lattice can be written, assuming a linear electron–phonon coupling, as follows:

$$\Delta E_S = \Delta E_S^0 + 2\hbar\omega_u \tanh(\hbar\omega_u/(2kT)) \tag{5}$$

with

$$\Delta E_S^0 = 2\sum \hbar\omega_i S_i . \tag{6}$$

In (5) the first term ΔE_S^0 is the Stokes shift for a parity-allowed transition and involves the Huang-Rhys factor of vibrational modes, Γ_i, which can be linearly coupled to the electronic excited state denoted as Γ_e. This coupling exists if $\Gamma_i \subset \Gamma_e \times \Gamma_e$. The second term in (5) accounts for the odd-phonon assistance required for a crystal-field band of an O_h MX_6 complex to become electric dipole allowed. In (5) $\omega_u/2\pi$ corresponds to the frequency of the odd mode giving rise to the main ED false origin. At low temperatures ($kT \ll \hbar\omega_u$) the second term increases ΔE_S^0 by a quantity equal to $2\hbar\omega_u$. It is worth noting that ΔE_S in (5) is the difference between the first moments of the absorption and the corresponding emission band [52].

For CrX_6^{3-} (X = F, Cl, Br) in cubic elpasolites [24 to 27] or VCl_6^{4-} in $CdCl_2$ and $MgCl_2$ [53] it has been shown [15] that coupling with two vibrational modes of the complex (a_{1g} as well as the Jahn-Teller mode e_g) explain ΔE_S^0 and the observed vibrational progressions. Therefore, ΔE_S^0 for these cases can be expressed as $\Delta E_S^0 = \Delta E_S^0(a_{1g}) + \Delta E_S^0(e_g)$.

For concentrated materials, where both migration and excitation trapping processes exist, the excitation and emission are not produced on equivalent ions and so the apparent Stokes shift can be written as

$$\Delta E_S^a = \Delta E_S + \Delta \tag{7}$$

where the trap depth, Δ, is involved in (4).

Using these ideas let us first discuss the experimental value $\Delta E_S^a = 3200\ cm^{-1}$ found for Na_6MnCl_8 at 10 K. In Section 2 it has been shown that both the vibrational progressions and the bandwidth of the $^4T_{1g}(G)$ band can be well explained through a coupling with practically only the a_{1g} mode and a value $S(a_{1g}) = 5$. Therefore, taking $\hbar\omega(a_{1g}) = 220\ cm^{-1}$ for the two observed progressions (Fig. 5a), we obtain $\Delta E_S(a_{1g}) = 2\hbar\omega_{a_{1g}} + \hbar\omega_{a_{1g}}/2 = 2310\ cm^{-1}$, which is $900\ cm^{-1}$ smaller than the experimental Stokes shift. Such an energy difference cannot be accounted for by invoking only odd-parity vibrations. Though couplings to these modes are needed for phonon-assisted ED transitions, their frequencies in $MnCl_6^{4-}$ are not high enough to overcome the difference of $900\ cm^{-1}$. An estimation of the odd-parity vibration frequencies in $MnCl_6^{4-}$ can be made from the lifetime measurements carried out in the 4 to 300 K range in NaCl: Mn^{2+}, Eu^{2+} crystals with isolated $MnCl_6^{4-}$ units [54]. These results indicate that τ decreases with temperature from $\tau = 44$ ms at 4 K down to 28 ms at 300 K, $\tau(T)$ behaving as $\tau(T) = \tau(0)\tanh(\hbar\omega_u/2kT)$ characteristic of assisted ED transitions, with an effective frequency $\hbar\omega_u = 300\ cm^{-1}$. Assuming the same frequency for the odd-parity vibrations in Na_6MnCl_8 and the transitions to be purely ED, the low-temperature Stokes shift should increase by about $600\ cm^{-1}$ which is still $300\ cm^{-1}$ below ΔE_S^a.

It is worth noting now that this difference, corresponding to $\Delta E_S^a - \Delta E_S^0(a_{1g}) - 2\hbar\omega_u$, is quite comparable to $\Delta = 350\ cm^{-1}$ obtained through the fitting of the experimental $\tau(T)$ curve to (4). This fact is thus in agreement with (7) and a much smaller coupling with the e_g mode as derived from the analysis of the $^4T_{1g}(G)$ bandwidth.

In the case of Na_6MnBr_8 the experimental ΔE_S^a value at 10 K is $3300\ cm^{-1}$. Taking $S(a_{1g}) = 8$, $\hbar\omega(a_{1g}) = 130\ cm^{-1}$, $\Delta = 480\ cm^{-1}$, and assuming $\hbar\omega_u \approx 200\ cm^{-1}$, a value $\Delta E_S^a = 3000\ cm^{-1}$ is obtained using (7). The difference of $300\ cm^{-1}$ between the latter value and the experimental one, $\Delta E_S^a = 3300\ cm^{-1}$, could reflect a small coupling with the e_g mode and thus $S(e_g)$ should be around 3 assuming $\hbar\omega_{e_g} \approx 100\ cm^{-1}$.

Therefore, the present analysis of the experimental Stokes shifts indirectly supports the idea that luminescence in Na_6MnX_8 (X = Cl, Br) is produced on a perturbed Mn^{2+} acting as a trap in the whole 2 to 300 K temperature range. This fact can now explain the absence of the vibrational structure in the luminescence spectrum even at 2 K, and also the larger bandwidth of emission bands when compared to the excitation ones. It can partially involve an inhomogeneous broadening on the emission band of the trap.

4.4 Mechanism of excitation transfer

Having in mind the preceding discussion, we consider the migration process. The transfer rate, P_{ab}, between two coupled Mn^{2+} ions, called α and β, one in the $^4T_{1g}(G)$ excited state and the other in the $^6A_{1g}(S)$ ground state is well described by the following general equation [55]:

$$P_{ab} = \frac{2\pi}{\hbar} |\langle a| H_{int} |b\rangle|^2 \int g_{ex}(E)\, G_{em}(E)\, dE\,, \tag{8}$$

where $|a\rangle = |^4T_{1g}^{\alpha}(G)\ ^6A_{1g}^{\beta}(S)\rangle$ and $|b\rangle = |^6A_{1g}^{\alpha}(S)\ ^4T_{1g}^{\beta}(G)\rangle$ are the initial and final pair states. H_{int} is the interaction Hamiltonian connecting both states, and g_{ex} and G_{em} are the normalized band shapes for the $^6A_{1g}(S) \leftrightarrow {}^4T_{1g}(G)$ excitation and emission transitions: $\int g_{ex}(E)\, dE = \int G_{em}(E)\, dE = 1$.

Let us consider as a first possible mechanism the so-called dipole–dipole interaction. In such a case, the correponding rate, P_{ab}^{DD}, is equal to [55]

$$P_{ab}^{DD} = \frac{3e^2 \varphi f \Omega}{4(2\pi n \tilde{\nu}_\Omega)^4 mc^2 \tau_0 R_{\alpha\beta}^6}, \tag{9}$$

where φ is the emission quantum efficiency for the donor, f the absorption oscillator strength for the acceptor, $\tilde{\nu}_\Omega$ the average wave number in the overlap between the normalized $g_{ex}(\tilde{\nu})$ and $G_{em}(\tilde{\nu})$, $\Omega = \int g_{ex}(\tilde{\nu})\, G_{em}(\tilde{\nu})\, d\tilde{\nu}$, τ_0 the radiative lifetime of the donor, and $R_{\alpha\beta}$ the distance between ions α and β.

The total probability of transfer, P^{DD}, should be that corresponding to a pair multiplied by the number of closest Mn^{2+} ions, $N = 12$. Therefore, assuming $\varphi = 1$, the relation between P^{DD} and the overlap Ω becomes

$$P^{DD} = 8.4 \times 10^3\, \Omega \tag{10}$$

for P^{DD} in s^{-1} and Ω in units of cm^{-1}.

For reaching this relation we have taken $\tau_0 = 70$ ms, corresponding to the low-temperature value for Na_6MnCl_8. From this a value $f = 2 \times 10^{-8}$ has been derived through the equation relating τ and f for ED transitions [43]. $\tilde{\nu}_\Omega$ has been taken equal to 18000 cm^{-1}.

Therefore, even putting the overlap $\Omega = 1.2 \times 10^{-5}$ cm^{-1}, as found at 300 K, (10) leads to a value $P^{DD} = 0.1$ s^{-1} which is about 100 times smaller than τ_0^{-1}. Therefore, an intrinsic luminescence would be observed provided dipole–dipole interactions were the mechanism for Mn^{2+}–Mn^{2+} transfer.

Let us now investigate whether an exchange process can be mainly responsible for an excitation transfer in our systems. As the $^4T_1(G)$ state is primarily made of the t^4e configuration, the transfer $|a\rangle \rightarrow |b\rangle$ requires conversion of a t electron in the α ion to an e one, while conversely an e electron of the β ion should become a t one. Within the superexchange theoretical framework [56, 57] this can be accomplished if we can build a molecular orbital (sometimes called magnetic orbital) involving both $|e^\alpha\rangle$ and $|t^\beta\rangle$ one-electron orbitals as well as an orbital for each one of the ligands encountered in the pathway. In the present case this can be accomplished easily because the direction joining two closest Mn^{2+} ions does not coincide with one of the principal directions of the octahedron. Fig. 7 depicts the atomic orbitals involved in a possible superexchange pathway. It can been seen that there is always a non-zero overlap between an atomic orbital and the adjacent one.

It is worth stressing now that excitation transfer through superexchange interactions does not need odd-phonon assistance in contrast to the dipole–dipole mechanism.

A rough estimation of the Mn^{2+}–Mn^{2+} transfer rate for Na_6MnCl_8 through exchange, P^{exch}, can be accomplished using the exchange constant $J = -0.017$ cm^{-1} corresponding to the ground state [5].

The pair exchange transfer rate, P_{ab}^{exch}, can be written as

$$P_{ab}^{exch} = \frac{2\pi}{\hbar} |\langle a| H_{exch} |b\rangle|^2\, \Omega^*, \tag{11}$$

where the effective exchange Hamiltonian is not detailed here and the overlap $\Omega^* \geqq \Omega$ does not include the phonon assistance.

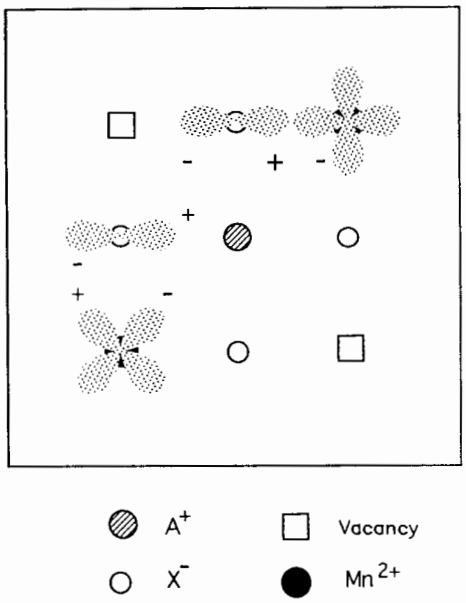

Fig. 7. Molecular orbital sketch showing the superexchange pathway between Mn^{2+} nearest neighbours in the Suzuki-phase structure. Note that a non-zero overlap between the $Mn^{2+}t_{2g}$ and e_g orbitals is possible through the p-orbitals of the Cl^- ligands drawn in the figure

Thus, taking into account the number of neighbours ($N = 12$) and assuming $\langle a|H_{exch}|b\rangle = -0.017\,cm^{-1}$, we obtain a rate (in s^{-1}) of

$$P^{exch} = 4.1 \times 10^9 \Omega^* , \tag{12}$$

for Ω^* in units of cm^{-1}. Therefore, even taking $\Omega^* = \Omega_0 = 2.9 \times 10^{-9}\,cm^{-1}$ observed at 10 K, P^{exch} becomes equal to $12\,s^{-1}$, which is comparable to the radiative rate, τ_0^{-1}.

In spite of the roughness of this estimate, the present model favours a rapid Mn^{2+}–Mn^{2+} transfer rate through superexchange, and so the experimentally observed $\tau(T)$ mainly accounts for much slower processes as the radiative emission at the trap, $\tau_R^*(T)$, and the corresponding non-radiative contribution, $\tau_{NR}^*(T)$, involving boiling off processes and the subsequent transfer to killers.

Further analysis of the present data, beyond the phenomenological behaviour contained in (4) requires an interpretation of the temperature dependence of the lifetime within our model.

Assuming that in our systems the energy transfer is diffusion limited, i.e. P_{MK} clearly higher than P_{MM} and P_{TM} (P_{TM}, P_{MM}, and P_{MK} being the transfer rates for trap $\rightarrow Mn^{2+}$, $Mn^{2+} \rightarrow Mn^{2+}$, and $Mn^{2+} \rightarrow$ killer, respectively), the time dependence of the trap luminescence intensity, $I(t)$, for a three-dimensional lattice in the $t \rightarrow \infty$ limit becomes [55]

$$I(t) = I_0 \exp\left[-(\tau_R^{-1} + 11.404 C_K C^{1/4} D^{3/4})\, t\right], \tag{13}$$

where τ_R is the radiative lifetime, C the parameter describing the Mn^{2+}–killer interaction (P_{MK}), D the diffusion constant connected with the migration (P_{MM} and P_{MT}), and C_K the killer concentration. If P_{MK} is clearly higher than P_{MM} and P_{TM}, on using (13), we are assuming a dipole–dipole interaction between Mn^{2+} and killers.

We stress that (13) is in perfect agreement with the present experimental observations where only low-temperature decays $I(t)$ slightly deviate from the exponential behaviour for $t < 8$ ms.

Let us now focus on explaining the $\tau(T)$ dependence using (13) from which $\tau^{-1}(T)$ can be written as $\tau_R^{*-1}(T) + \tau_{NR}^{*-1}(T)$, with

$$\tau_R^{*-1}(T) = \tau_R^{*-1}(0) \coth\left(\frac{\hbar\omega_u}{2kT}\right) \tag{14}$$

and

$$\tau_{NR}^{*-1}(T) = 11.4 C_K C^{1/4} D^{3/4} . \tag{15}$$

The temperature dependence of τ^*_{NR} mainly comes from the diffusion coefficient D, proportional to the transfer rate and is, therefore, proportional to the overlap Ω^*. This overlap can be calculated analytically for Gaussian shapes as a function of the separation, ΔE^*, between maxima of emission and absorption bands involved in the Mn^{2+}–Mn^{2+} transfer process, as well as of the halfwidth of the absorption band, $H_{1/2}$. The result is

$$\int g_{ex}(E)\, G_{em}(E)\, dE \propto \exp\left[-\frac{\ln 2}{2}\left(\frac{\Delta E^*}{H_{1/2}(T)}\right)^2 \right]. \tag{16}$$

In the case of Na_6MnCl_8, the temperature dependence of the halfwidth follows $H_{1/2}(T) = H_{1/2}(0)\,[\coth(\hbar\omega_{eff}/2kT)]^{1/2}$, with $\hbar\omega_{eff} = 214\ cm^{-1}$ (Fig. 3b). So that $\tau^{-1}(T)$ would be

$$\tau^{-1}(T) = \tau_R^{-1}(0) \coth\left(\frac{\hbar\omega_u}{2kT}\right) + A \exp\left[-\frac{3}{4}\frac{\ln 2}{2}\left(\frac{\Delta E^*}{H_{1/2}(0)}\right)^2 \tanh\left(\frac{\hbar\omega_{eff}}{2kT}\right)\right]. \tag{17}$$

Though the Gaussian approximation is not very accurate for low-temperature spectra, it reasonably reproduces the band shape for intermediate and high temperatures.

Fig. 6b shows the calculated $\tau(T)$ curve using the following fit parameters: $[\Delta E^*/H_{1/2}(0)]^2 = 24$, $\tau_R^{-1}(0) = 7.8\ s^{-1}$, and $A = 3500\ s^{-1}$. These values clearly point out that the transfer rate to killers is relevant even at $T = 2$ K, $\tau_{NR}^{-1}(2\ K) = 6.8\ s^{-1}$, and therefore the absence of vibronic structure in the luminescence spectrum at low temperatures due to inhomogeneous broadening is now justified. In fact, the Stokes shift derived from the value $\Delta E^*/H_{1/2}(0) = 4.9$ is $\Delta E^* = 2700\ cm^{-1}$ for $H_{1/2}(0) = 550\ cm^{-1}$. The separation, ΔE^*, obtained through this analysis is clearly smaller than that corresponding to experimental optical absorption and emission sidebands, $\Delta E_S = 3200\ cm^{-1}$. This fact is again fully consistent with (5) pointing out the necessity of phonon assistance in both optical absorption and emission processes. By contrast, in the transfer process induced by superexchange this is unnecessary and so ΔE^* should be close to $\Delta E_S - 2\hbar\omega_u$. As this is experimentally true, it provides a significant support to the transfer mechanism and also to the interpretation of the experimental $\tau(T)$ curve (Fig. 4) through the temperature dependence of Ω^*.

Before ending this section let us mention that though (13) has been derived for a dipole–dipole transfer mechanism between Mn^{2+} and killers, only the exponent 3/4 of the diffusion coefficient appears in the exponent of the second term in (17). Such an exponent is, however, likely to be not influenced by the kind of mechanism.

5. Final Comments

A main conclusion of the present work is the extrinsic character of the luminescence in Na_6MnX_8 microcrystals even at 2 K. It has been suggested that migration is strongly related to the separation, Δ_e, between the two first sublevels of the manifold $^4T_{1g}(G)$ state split by low symmetry fields, spin–orbit coupling, and exchange fields [20, 45]. In fact, at 0 K the only resonant Mn^{2+}–Mn^{2+} transfer process involves a deexcitation energy of a Mn^{2+} ion equal to the zero-phonon energy and the corresponding capture by the second one. However, for Δ_e values smaller than about 5 cm^{-1}, new resonant transfer channels can become active for $T \geqq 2$ K. In the absence of exchange fields associated to magnetic ordering, small Δ_e values are favoured by (i) a cubic symmetry and (ii) low values of the spin–orbit splitting.

The first condition is fully verified for Na_6MnX_8 compounds and explains qualitatively why luminescence is extrinsic in the present case while intrinsic up to ≈ 100 K for $RbMnCl_3$ where $\Delta_e = 537\,cm^{-1}$ [45]. As regards the spin–orbit coupling constant it can be substantially quenched because of the Jahn-Teller effect in the $^4T_{1g}(G)$ excited state even neglecting the reduction due to covalency. The Ham reduction factor, γ, of the spin–orbit interaction can be written as a function of the Huang-Rhys factor, $S(e_g)$, as $\gamma = \exp[-\frac{3}{2}S(e_g)]$. In view of the analysis carried out in Sections 4.1 and 4.3 upon both the experimental Stokes shift and the $^4T_{1g}(G)$ bandwidth, a value $S(e_g) \approx 2$ would be expected for these systems. This would give rise to a separation of $\approx 3\,cm^{-1}$ between the two lowest sublevels arising from the $^4T_{1g}(G)$ state.

The presence of a small coupling to the e_g mode is particularly clear for Na_6MnBr_8. Furthermore, the true separation between the four states arising from the $^4T_{1g}(G)$ because of the spin–orbit coupling has been measured in Mn^{2+}-doped fluoroperovskites by highly resolved emission spectra at 5 K. The splitting observed between the two lowest spinors, $9\,cm^{-1}$ for $KMgF_3:Mn^{2+}$ and $7\,cm^{-1}$ for $KZnF_3:Mn^{2+}$, is consistent with values $S(e_g) = 1.4$ and 1.5, respectively [19]. This splitting was not observed in the low-temperature emission spectra of Mn^{2+}-doped $RbCdF_3$, $RbCaF_3$, and $CsCaF_3$ [58], thus meaning higher values of $S(e_g)$. The values $S(e_g) \geqq 2$ for Na_6MnX_8 (X = Cl, Br) are consistent with the fact that the replacement of F^- by another less electronegative ligand (like Cl^- or Br^-) tends to increase the Huang-Rhys factors [37, 58].

The present conclusions about the vibronic coupling to the modes of the MnX_6^{4-} complex disagree with those reached by Ronda et al. [59] for $MnCl_2$ and $MnBr_2$. In fact, though no vibrational progression was observed in the $^4T_{1g}(G)$ band, they determined the $S(e_g)$, $S(a_{1g})$, $\hbar\omega(a_{1g})$ and $\hbar\omega(e_g)$ values by fitting only the low-temperature bandwidths and their temperature dependences. This procedure leads to a ratio $S(e_g)/S(a_{1g})$ of 4.9 and 1.9 for $MnCl_2$ and $MnBr_2$, respectively.

A final point to be analyzed is the different shift experienced by the emission and the $^4T_{1g}(G)$ excitation peaks from 10 to 300 K. Designating such shifts by δE_E and δE_A, respectively, it has been found $\delta E_E = 600\,cm^{-1}$ and $\delta E_A = 150\,cm^{-1}$ for Na_6MnCl_8, and $\delta E_E = 530\,cm^{-1}$ and $\delta E_A = 250\,cm^{-1}$ for Na_6MnBr_8. The higher variation of the emission could be partially accounted for if the transition involves phonon-assistance by odd vibrational modes. In such a case, the excitation and emission band maxima are given by

$$E_A = E_{ZPL} + \frac{1}{2}\Delta E_S^0 + \hbar\omega_u \tanh\left(\frac{\hbar\omega_u}{2kT}\right) \tag{18}$$

and

$$E_E = E_{ZPL} - \frac{1}{2}\Delta E_S^0 - \hbar\omega_u \tanh\left(\frac{\hbar\omega_u}{2kT}\right) - \Delta\,, \tag{19}$$

where E_{ZPL} is the zero-phonon line energy. These relations lead to the expressions for the Stokes shift, ΔE_S^a, given in (7). For intrinsic luminescence, $\Delta = 0$, the Stokes shift is just as given in (5). The simplifying assumptions involved in (18) and (19) are (i) only one odd mode is considered, and (ii) its frequency is the same for normal and perturbed Mn^{2+}. Therefore, neglecting in a first approximation the shifts undergone by ΔE_S^0 and Δ in the 10

to 300 K range, δE_A and δE_E are calculated to be

$$\delta E_A \equiv E_A(T^*) - E_A(10\text{ K}) = \delta E_{ZPL} - \hbar\omega_u\left(1 - \tanh\left(\frac{\hbar\omega_u}{2kT^*}\right)\right) \tag{20}$$

and

$$\delta E_E \equiv E_E(T^*) - E_E(10\text{ K}) = \delta E_{ZPL} + \hbar\omega_u\left(1 - \tanh\left(\frac{\hbar\omega_u}{2kT^*}\right)\right), \tag{21}$$

where $T^* = 300$ K.

The positive signs of both δE_A and δE_E found experimentally reflect the blue shift experienced by the zero-phonon line upon warming. This is consistent with the decrease undergone by $10Dq$ and the subsequent increment of E_{ZPL}. A full discussion of this point for Mn^{2+} fluoroperovskites will be reported later [58].

From (20) and (21) we get

$$\delta E_E - \delta E_A = 2\hbar\omega_u\left(1 - \tanh\left(\frac{\hbar\omega_u}{2kT^*}\right)\right). \tag{22}$$

This mechanism leads to differences $\delta E_E - \delta E_A \approx 230\text{ cm}^{-1}$ using $\hbar\omega_u$ values ranging from 200 to 300 cm^{-1}. Though this difference is close to that found for Na_6MnBr_8, $\delta E_E - \delta E_A = (280 \pm 120)\text{ cm}^{-1}$, a proper comparison between these values cannot be made because the luminescence at 300 K comes from a different trap. In the case of Na_6MnCl_8, this mechanism accounts for half the experimental value, $\delta E_E - \delta E_A = (450 \pm 120)\text{ cm}^{-1}$.

A further study on other systems containing $MnCl_6^{4-}$ units becomes desirable for clarifying this point. Work in this direction is now under way.

Acknowledgement

This work has been supported by the CICYT under project No. PB 92-0505.

References

[1] K. SUZUKI, J. Phys. Soc. Japan **16**, 67 (1961).
[2] J. A. CHAPMAN and E. LILLEY, J. Mater. Sci. **10**, 1154 (1975).
[3] M. YACAMÁN, L. W. HOBBS, and M. J. GORINGE, phys. stat. sol. (a) **39**, K85 (1977).
[4] F. RODRÍGUEZ, J. C. GOMEZ SAL, M. MORENO, A. DE GEYER, and C. JANOT, Phys. Rev. B **43**, 7519 (1991).
[5] M. MORENO, J. C. GOMEZ SAL, J. A. ARAMBURU, F. RODRÍGUEZ, J. L. THOLENCE, and F. JAQUE, Phys. Rev. B **29**, 4192 (1984).
[6] J. C. GOMEZ SAL, F. RODRÍGUEZ, M. MORENO, and J. L. THOLENCE, Phys. Rev. B **37**, 454 (1988).
[7] J. C. GOMEZ SAL, M. MORENO, F. RODRÍGUEZ, A. RAVEX, and J. L. THOLENCE, J. Phys. C **20**, L421 (1987).
[8] A. DE ANDRES, J. M. CALLEJA, F. FLORES, V. R. VELASCO, and E. LILLEY, J. Phys. Chem. Solids **41**, 1367 (1980).
[9] F. AGULLO-LOPEZ, J. M. CALLEJA, F. CUSSÓ, F. JAQUE, and F. J. LOPEZ, Progr. Mater. Sci. **39**, 187 (1986).
[10] F. RODRÍGUEZ, M. MORENO, F. JAQUE, and F. J. LOPEZ, J. chem. Phys. **78**, 1 (1983).
[11] F. JAQUE, F. J. LOPEZ, F. CUSSO, F. MESSEGUER, F. AGULLO-LOPEZ, and M. MORENO, Solid State Commun. **47**, 103 (1983).
[12] M. MORENO, F. RODRÍGUEZ, J. A. ARAMBURU, F. JAQUE, and F. J. LOPEZ, Phys. Rev. B **28**, 6100 (1983).
[13] A. DE ANDRES, J. M. CALLEJA, I. POLLINI, and G. BENEDEK, Inorg. Chem. **143**, 71 (1986).

[14] M. C. Marco de Lucas, F. Rodríguez, and M. Moreno, J. Phys.: Condensed Matter **2**, 1981 (1990).
[15] M. Moreno, M. T. Barriuso, and J. A. Aramburu, J. Phys.: Condensed Matter **4**, 9481 (1992).
[16] M. C. Marco de Lucas and F. Rodríguez, Rev. sci. Instrum. **61**, 23 (1990).
[17] P. J. Alonso and R. Alcala, J. Lum. **22**, 321 (1981).
[18] V. Goldberg, R. Moncorge, D. Pacheco, and B. di Bartolo, in: Luminescence of Inorganic Solids, Ed. B. Di Bartolo, Plenum Press, New York 1988.
[19] F. Rodríguez, H. Riesen, and H. U. Gudel, J. Lum. **50**, 101 (1991).
[20] B. Wilson, W. Yen, J. Hegarty, and G. Imbusch, Phys. Rev. B **19**, 4238 (1979).
[21] J. B. Bates, R. F. Wood, G. E. Shankle, and M. Mostoller, Phys. Rev. B **6**, 3267 (1977).
[22] A. de Andres and J. M. Calleja, Solid State Commun. **48**, 11 (1983).
[23] E. I. Solomon and D. S. McClure, Phys. Rev. B **9**, 4690 (1974).
[24] H. U. Gudel and T. R. Snellgrove, Inorg. Chem. **17**, 1617 (1978).
[25] P. Greenough and A. G. Paulusz, J. chem. Phys. **70**, 1967 (1979).
[26] L. Dubicki, J. Ferguson, and B. von Oosterhout, J. Phys. C **13**, 2791 (1980).
[27] M. C. Marco de Lucas, F. Rodríguez, and M. Moreno, J. Lum. **48/49**, 553 (1991).
[28] I. Pollini, G. Spinollo, and G. Benedek, Phys. Rev. B **22**, 6369 (1980).
[29] P. J. McCarthy and H. U. Gudel, Inorg. Chem. **25**, 838 (1986).
[30] P. J. McCarthy and H. U. Gudel, Inorg. Chem. **23**, 880 (1984).
[31] F. Agullo-Rueda, J. M. Calleja, F. Jaque, J. D. Tornero, and F. Palacio, Solid State Commun. **60**, 331 (1986).
[32] D. H. Good, J. chem. Phys. **43**, 2830 (1965).
[33] K. Pierloot, E. van Praet, and L. G. Vanquickenborne, J. chem. Phys. **96**, 4163 (1992).
[34] J. A. Aramburu, private communication.
[35] H. G. Drickamer and C. W. Franck, in: Electronic Transitions and the High Pressure Chemistry and Physics of Solids, Chapman & Hall, London 1973.
[36] D. Gerlich, S. Hart, and D. Whittal, Phys. Rev. B **29**, 2142 (1984).
[37] R. Knochenmuss, C. Reber, M. V. Rajasekharan, and H. U. Gudel, J. chem. Phys. **85**, 4280 (1986).
[38] P. S. May and H. U. Gudel, J. Lum. **46**, 277 (1990).
[39] R. Alcala, J. Casas Gonzalez, B. Villacampa, and P. J. Alonso, J. Lum. **48/49**, 569 (1991).
[40] L. J. Andres, A. Lempicki, B. C. Collum, C. J. Giunta, R. H. Bartram, and J. F. Dolan, Phys. Rev. B **34**, 2735 (1986).
[41] C. Reber, H. U. Gudel, G. Meyer, T. Scheild, and C. A. Daul, Inorg. Chem. **28**, 3249 (1989).
[42] M. D. Sturge, Phys. Rev. B **8**, 6 (1973).
[43] B. Henderson and G. F. Imbusch, in: Optical Spectroscopy of Inorganic Solids, Oxford University Press, New York 1989.
[44] F. Rodríguez, M. Moreno, J. Baruchel, and J. Y. Henry, J. Physique **46**, C7–155 (1985).
[45] U. Kambli and H. U. Gudel, Inorg. Chem. **23**, 3479 (1984).
[46] T. Tsuboi, P. Silfsten, and K. Iio, phys. stat. sol. (b) **170**, K55 (1992).
[47] F. Rodríguez and M. Moreno, Solid State Commun. **58**, 701 (1986).
[48] F. Rodríguez and M. Moreno, J. Physique **46**, C7–151 (1985).
[49] M. C. Marco de Lucas, F. Rodríguez, and M. Moreno, phys. stat. sol. (b) **172**, 719 (1992).
[50] F. Rodríguez, M. Moreno, J. M. Dance, and A. Tressaud, Solid State Commun. **69**, 67 (1989).
[51] M. C. Marco de Lucas, F. Rodríguez, and M. Moreno, J. Phys.: Condensed Matter, in the press.
[52] J. Bourgoin and M. Lannoo, in: Point Defects in Semiconductors II, Springer-Verlag, Berlin 1983.
[53] B. Galli, A. Hauser, and H. U. Gudel, Inorg. Chem. **24**, 2271 (1985).
[54] R. Cywiński, E. Mugeński, and I. Sokóska, phys. stat. sol. (b) **157**, 137 (1990).
[55] L. C. Powell and G. Blasse, in: Luminescence and Energy Transfer, Structure and Bonding, Vol. 42, Springer-Verlag, Berlin 1980.
[56] P. J. Hay, J. C. Thibeault, and R. Hoffmann, J. Amer. Chem. Soc. **97**, 4884 (1975).
[57] P. W. Anderson, Solid State Phys. **14**, 99 (1963).
[58] M. C. Marco de Lucas, Thesis Dissertation, University of Cantabria, 1992.
[59] C. R. Ronda, H. H. Siekman, and C. Haas, Physica (Utrecht) **144B**, 331 (1987).

(Received February 15, 1994)